Check for updates

Effects of Sm on Fe–Mn catalysts for Fischer–Tropsch synthesis†

Zhonghao Han,[a] Weixin Qian,[a] Hongfang Ma,[a] Haitao Zhang,[a] Qiwen Sun[b] and Weiyong Ying [ID] *[a]

Sm-promoted FeMn catalysts were prepared by the co-precipitation method and characterized by N_2 adsorption, XRD, CO-TPD, H_2-TPD, CO_2-TPD, H_2-TPR, XPS and MES. It was found that compared with the un-promoted catalyst, when Sm was added at a proper content, the catalyst showed a larger BET surface area and promoted the formation of iron particles with a smaller size. The presence of Sm could increase the surface charge density of iron, which enhanced the Fe–C bond and promoted the stability and amount of CO dissociated adsorption, as confirmed by XPS and CO-TPD. Furthermore, according to MES, Sm could promote the formation of Fe_5C_2, which was the active phase of FTS. In addition, Sm could also enhance the basicity of the catalysts and suppress the H_2 adsorption capacity, which inhibited the hydrogenation reaction and the conversion of olefins to paraffins, as verified by the results of CO_2-TPD and H_2-TPD. According to the FTS performance results, compared with the observations for the un-promoted catalysts, when the molar ratio of Sm to Fe was 1%, the CO conversion increased from 63.4% to 70.4%, the sum of light olefins in the product distribution increased from 26.6% to 32.6, and the ratio of olefins to paraffins increased to 4.18 from 4.09.

1. Introduction

Due to the shortage of fossil energy and the increasingly severe environmental problems, Fischer–Tropsch synthesis (FTS) has aroused much attention[1] as it can convert syngas into raw oil and chemicals without sulfur, nitrogen and aromatic hydrocarbons.[2] Many studies have shown that only iron and cobalt catalysts have the value of being industrialized.[3] Cobalt-based catalysts have higher FTS activity as well as higher selectivity of high-carbon hydrocarbons and paraffins.[4] Compared to cobalt-based catalysts, iron-based catalysts are attractive for their high water gas shift (WGS) and high CO_2 selectivity due to the Boudouard mechanism.[5,6]

In the Fischer–Tropsch synthesis, many metals have been introduced as promoters. The impact of the Group I alkali metals upon the activity of the iron catalysts was studied and it was found that potassium promotion provided an outstanding catalyst at the activity viewpoint for both the FTS and WGS reactions.[7] Other research studies suggested that all Group II metal promoters yielded similar carbon utilization but with higher alpha values than that of an unpromoted catalyst in FTS.[8,9] It is generally believed that manganese promoters in iron-based catalysts are beneficial for the formation of low-carbon olefins for FTS.[10] The reason for this finding may be that manganese can enhance the adsorption capacity of CO and promote the formation of iron carbide.[11] The study showed that the Mn promoter was beneficial for the formation of light carbon olefins.[12,13] Some studies have shown that the introduction of Mn as a structure promoter into iron-based catalysts for the Fischer–Tropsch synthesis can enhance the stability of catalysts and promote the WGS reaction.[14,15] In contrast, other reported Mn promoters enhanced the selectivity of olefins and C_{5+} but restrained the selectivity of methane.[16,17] In addition, some studies have shown that structural promoters such as SiO_2,[18,19] Al_2O_3 [20] and TiO_2 can improve the selectivity, activity and stability of iron-based catalysts.[21]

In recent years, rare earth metals have been reported as promoters. The catalytic performance of the precipitated Fe–Cu catalyst promoted with La, Ce, Nd, Eu and Th oxides was investigated and the results showed that rare earth metal oxides and Th promoters could increase the dispersion and stabilization of the iron-based catalysts, inhibiting their growth and further reduction.[22] Some studies suggest that the introduction of a small amount of rare earth metal will greatly increase the performance of iron-based catalysts, but excessive rare earth metal promoters will significantly inhibit FTS.[23,24] The effect of La_2O_3 on a precipitated iron catalyst showed that the addition of

[a]Engineering Research Center of Large Scale Reactor Engineering and Technology, Ministry of Education, State Key Laboratory of Chemical Engineering, East China University of Science and Technology, Shanghai 200237, China. E-mail: wying@ecust.edu.cn; Fax: +86 21 64252192; Tel: +86 21 64252151

[b]State Key Laboratory of Coal Liquefaction and Coal Chemical Technology, Shanghai 201203, China

La_2O_3 increased the formation of methane while suppressing the selectivity for C_5^+ hydrocarbons.[25]

Although many rare earth metal promoters have been studied, few studies have been performed with samarium as promoters. The aim of this work was to investigate the influence of samarium upon the properties of iron-based catalysts in the FTS reaction. Iron-based catalysts modified by samarium were prepared by the co-precipitation method and tested under FTS conditions in a fixed tube reactor to analyse the promotion effect of samarium on the activity and product distribution. The influences of Sm_2O_3 on the structure, adsorption properties, reduction properties and FTS catalytic performance of the iron-based catalysts were researched *via* N_2 adsorption, XRD, CO-TPD, H_2-TPD, CO_2-TPD, H_2-TPR, XPS and Mössbauer spectroscopy.

2.   Experimental

2.1.   Catalyst preparation

The Sm-promoted catalysts were prepared by the co-precipitation method. A solution containing iron(III) nitrate nonahydrate (>99.99 wt% Shanghai Macklin Biochemical Co., Ltd), manganese nitrate (50 wt% Shanghai Macklin Biochemical Co., Ltd) and samarium(III) nitrate hexahydrate (>99.99 wt% Shanghai 3A Chemical Co., Ltd) with the desired ratio was precipitated by anhydrous sodium carbonate (>99.99 wt% Shanghai Macklin Biochemical Co., Ltd) at 65 °C. The pH value of the solution was kept at 8.0 ± 0.3. Then, the solution was stirred for 0.5 h and aged for 1 h. After washing, filtration and drying, the precipitate was treated at 550 °C for 3 h. The FeMnSm catalysts were prepared by the above methods. The molar compositions of the catalysts were 100Fe/10Mn/xSm (x = 0, 0.5, 1, 1.5 and 2), which were labeled as Sm0, Sm0.5, Sm1, Sm1.5 and Sm2, respectively.

2.2.   Catalyst characterization

N_2 physical adsorption was performed at 77 K with a Micromeritics ASAP 2020 instrument. The samples were evacuated at 120 °C for 4 h before the adsorption measurement. Specific surface areas were measured using the Brunauer Emmett Teller (BET) method. Pore volumes and pore sizes were measured by the Barrett–Joyner–Halenda (BJH) procedure.

The XRD patterns of the samples were obtained on a diffractometer operating with Cu Kα radiation at 40 kV with a scanning rate of 6° min^{-1} and 2θ angles ranging from 10 to 80°.

CO-TPD, H_2-TPD and CO_2-TPD were carried out using a Micromeritics Autochem 2920 apparatus with a thermal conductivity detector (TCD). About 100 mg samples were reduced under an H_2 flow at 350 °C for 2 h and were cooled to 60 °C under an He gas flow. Afterwards, $CO/H_2/CO_2$ were introduced into the catalyst bed for 30 min. Then, the catalyst bed was purged by the flow for 60 min. Subsequently, the samples were heated to 800 °C at a rate of 10 °C min^{-1}. The desorbed products were detected with the TCD detector.

H_2-TPR of the fresh catalysts was carried out in a conventional atmospheric quartz flow reactor by a Micromeritics ASAP 2920 instrument. About 50 mg catalysts were purged in a flow of argon at 350 °C for 2 h and then cooled to 50 °C. Each sample was treated in 10% H_2/90% Ar (v/v) at a flow rate of 50 ml min^{-1}, and the reduction temperature was increased from room temperature to 800 °C at a rate of 10 °C min^{-1}.

X-ray photoelectron spectroscopy (XPS) was performed on a VG ESCALAB 250Xi electron spectrometer equipped with a hemispherical analyzer operating in a constant pass energy mode and an Al Kα X-ray source operating at 10 mA and 12 kV. The samples were reduced by H_2 at 350 °C and 0.1 Mpa for 10 h before the measurement. The reduced catalysts were placed in nitrogen to avoid oxidation.

Mössbauer spectroscopy (MES) of the catalyst samples was performed on an MR-351 constant-acceleration Mössbauer spectrometer (FAST, Germany) at room temperature with ^{57}Co in a Pd matrix. The spectra were collected over 512 channels in the mirror image format. The Mössbauer parameters including an isomer shift (IS), quadruple splitting (QS), and hyperfine field (Hhf) were used to identify the components of the iron phase. The reacted catalysts were placed in nitrogen to avoid oxidation.

2.3.   FTS performance

The FTS performance of the catalysts was conducted in a fixed bed reactor (ID = 10 mm). The detailed description of the reactor and the product analysis system has been provided elsewhere.[26] The particle size of the catalysts was 60–80 mesh, and 0.3 g of the catalyst sample was mixed with 0.6 g of the same particle sized quartz grains. The catalysts were reduced with H_2 at 350 °C, 0.10 MPa and GHSV 4000 ml g^{-1} h^{-1} for 10 h. The FTS catalyst activity tests were maintained at 300 °C, 1.0 MPa, H_2/CO = 2 and 12 000 ml g^{-1} h^{-1}. After the FTS reaction, the outlet gases CO, H_2, CH_4, *etc.* were analyzed by online GC Agilent 7890A with a thermal conductivity detector (TCD). The waxes were dissolved in CS_2 and detected off-line by GC Agilent 7890A with a flame ionization detector (FID).

3.   Result and discussion

3.1.   Catalyst characterization

3.1.1.   Textural properties of catalysts. The textural and structural properties of the corresponding catalysts were characterized by N_2 physical adsorption and XRD. The N_2 physical adsorption–desorption isotherms of the FeMnSm catalysts are shown in Fig. 1. No significant increase in the catalysts was detected after N_2 uptake until the relative pressure (P/P_0) increased to 0.9. A rapid increase was seen when P/P_0 was beyond 0.9. Therefore, the existence of a larger mesoporous and intergranular pore space was proven.[27] During FTS, these characteristics were helpful to reduce the mass transfer resistance and shorten the residence time of the feed gas, thereby promoting the formation of low-carbon hydrocarbons and inhibiting the formation of high-carbon hydrocarbons.[28]

The BET surface areas, pore volumes and pore sizes of the fresh catalysts with various samarium contents are listed in Table 1. It can be seen that the BET surface areas of the catalysts first increase with the increase in samarium from 0 to 1%. This
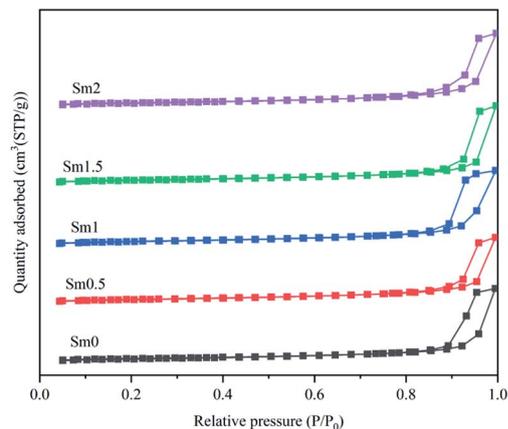
Fig. 1 N$_2$ physical adsorption–desorption isotherms of the FeMnSm catalysts.
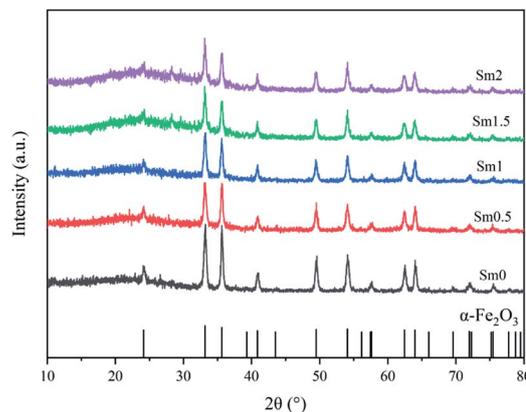

Fig. 2 XRD patterns of the FeMnSm catalysts with different Sm loadings.

result can be due to the fact that the introduction of a small amount of rare earth metal promoters can increase the dispersion of iron atoms. With the continuous increase in the Sm promoter content from 1% to 2%, the specific surface area of the catalyst decreased, which indicated that rare earth oxides partly blocked the pore path of the catalysts. This may reduce the activity of the catalysts.

The X-ray powder diffraction patterns of fresh catalysts with different Sm loadings are shown in Fig. 2. All the fresh catalysts with different Sm contents showed the characteristic peaks of α-Fe$_2$O$_3$, which had a characteristic structure with 2θ values of 24.2, 33.2, 35.7, 40.9, 49.5, 54.1, 57.7, 62.5, and 64.1°; the XRD pattern of hematite Fe$_2$O$_3$ according to JCPDS #99-0060 is shown at the bottom of Fig. 2. On increasing the Sm content from 0 to 1%, the intensity of these peaks showed a decreasing trend, which indicated that the crystallinity of the iron phases became poor with the addition of samarium. The crystallite sizes of Fe$_2$O$_3$ were calculated by the Scherrer's equation according to the full spectrum data and are listed in Table 1. Therefore, Sm could maintain high dispersion of iron particles.

3.1.2. Desorption and reduction properties of catalysts. The results of CO-TPD are shown in Fig. 3. The peak temperature and desorption amount are shown in Table S1.† Two desorption peaks could be observed for all samples. According to previous studies,[29] the low temperature peak at about 85 °C is related to the molecular adsorption of CO and the high temperature peak beyond 550 °C can be assigned to the

dissociated adsorption of CO.[30] No significant difference was observed for the lower desorption peaks, showing that Sm had little effect on the CO molecular adsorption. However, obvious differences could be observed for the high temperature desorption peaks. When the Sm content increased from 0 to 1%, the peaks shifted to a higher temperature zone and the area increased, which indicated that both the CO desorption temperature and desorption amount increased. This was because Sm can be considered as a promoter, which can donate its electrons to iron atoms; this can lead to an increase in the surface charge density of the iron atoms, contributing to the adsorption of CO and the formation of the Fe–C bonds.[31,32] However, both the desorption temperature and area decreased when the Sm content continued to increase from 1% to 2%, indicating that excessive Sm was not conducive to CO adsorption. According to the BET result, this probably resulted from the fact that Sm covered the active sites of the catalyst, blocking the channels of the catalyst and occupying the active sites of the catalyst, which reduced the adsorption of CO on the iron catalyst.

The results of H$_2$-TPD are shown in Fig. 4. The peak temperature and desorption amount are shown in Table S2.† It

Table 1 Result of the N$_2$-physisorption for the fresh catalysts

Catalyst	S_{BET} (m^2 g^{-1})	$D_p{}^a$ (nm)	$V_P{}^b$ (cm^3 g^{-1})	$D_{Fe}{}^c$ (nm)
Sm0	22.8	23.5	0.18	18.0
Sm0.5	25.2	22.0	0.19	17.9
Sm1	26.7	20.9	0.18	16.1
Sm1.5	23.5	21.5	0.16	16.4
Sm2	23.0	22.8	0.18	16.9

^{a} BJH desorption average pore size. ^{b} BJH desorption pore volume. ^{c} Calculated by the Scherrer equation according to the results of XRD.
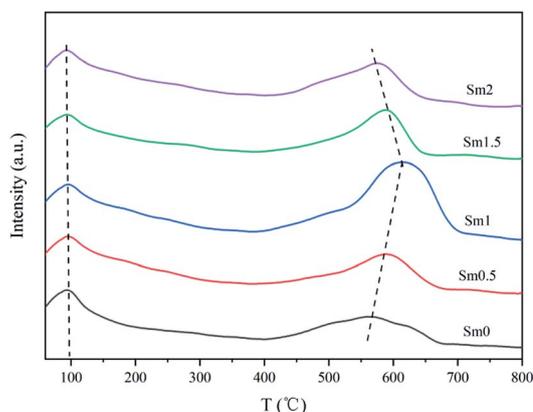

Fig. 3 CO-TPD patterns of the FeMnSm catalysts with different Sm loadings.

can be seen that the H_2-TPD patterns of all the catalysts contain two desorption peaks. The first one lower than 100 °C corresponds to the weakly adsorbed H species on the iron-based catalyst surface.[33] The second peak in the range of 240–290 °C was ascribed to the strongly chemically adsorbed hydrogen on the deep sites of the iron surface.[34] When the Sm content increased from 0 to 2%, the desorption peak in the low temperature zone hardly changed, indicating that Sm had no obvious effect on the low temperature adsorption of H_2 on the catalysts. On the other hand, the desorption amount of sample Sm1 in high temperature zone is the smallest. This was because the addition of an appropriate amount of Sm increased the charge density of Fe, which inhibited the formation of the Fe–H bond and weakened the adsorption of H_2.[35]

CO$_2$-TPD was performed to get information about the surface basicity of the FeMnSm catalysts, as shown in Fig. 5. The peak temperature and desorption amount are shown in Table S3.† The CO$_2$-TPD profiles of the FeMnSm catalysts could be divided into one desorption peak at a lower temperature (100 °C) and one peak at a higher temperature (450–550 °C). The first peak at about 100 °C could be contributed by weakly absorbed CO$_2$ on the surface of the catalysts. The second one corresponded to the desorption of the strongly chemisorbed CO$_2$. When the Sm content increased from 0 to 1%, the chemical adsorption peak area and desorption temperature increased significantly, showing that the basicity of the catalyst increased. However, when the Sm content continued to increase to 2%, the low temperature adsorption of CO$_2$ increased and the strong adsorption decreased, proving that when Sm exceeded the appropriate value, the basicity of the catalyst decreased and the adsorption of CO$_2$ changed from chemical adsorption to physical adsorption. A possible reason could be that the catalyst surfaces were covered and the active sites binding to CO$_2$ were reduced.

The H_2-TPR profiles of the catalysts are shown in Fig. 6. Three obvious reduction peaks can be observed. The first peak between 250 and 300 °C represents α-Fe$_2$O$_3$ → Fe$_3$O$_4$. The second peak between 400 and 500 °C corresponds to the Fe$_3$O$_4$ → FeO process. The last peak over 600 °C represents FeO → α-
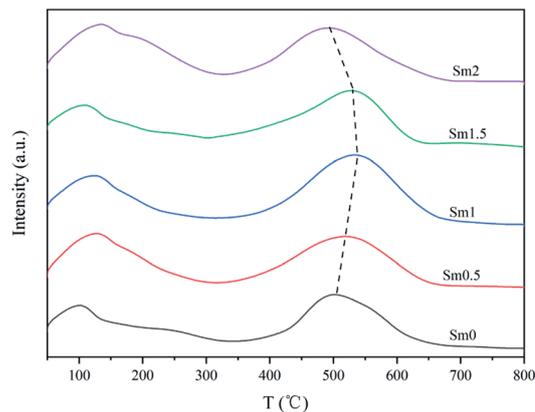

Fig. 5 CO$_2$-TPD patterns of the FeMnSm catalysts with different Sm loadings.

Fe. The FeO phase was unstable below 590 °C. Therefore, Fe$_3$O$_4$ was partially reduced to α-Fe, and the remaining species were reduced to FeO.[36] It is generally believed that the Fe species in the catalyst during reduction and reaction undergo the following transformation: Fe$_2$O$_3$ → Fe$_3$O$_4$ → Fe$_5$C$_2$.[37] By comparing the first reduction peak of the sample, it can be found that the peak temperature decreased when Sm increased from 0 to 1%, indicating that the introduction of samarium into the iron-based catalyst enhanced the reduction process of α-Fe$_2$O$_3$ to Fe$_3$O$_4$.[38] Nevertheless, when the Sm content continued to increase to 2%, the reduction peak temperature increased, indicating that the addition of excessive Sm was disadvantageous to catalyst reduction.

3.1.3. Electronic effect of Sm promoter. The Fe 2p spectra of the catalysts named Sm0, Sm0.5 and Sm1 after reduction are displayed in Fig. 7 and the molar ratios of the surface elements are listed in Table S4.† Two main peaks located at about 710.9 eV and 724.7 eV were attributed to Fe 2p3/2 and Fe 2p1/2, respectively.[39] The electronegativity data showed that Fe (1.83) > Sm (1.17). The greater the electronegativity, the stronger the ability of the atoms to attract electrons. According to the result of XPS, both the peaks shifted to lower binding energy for the Fe
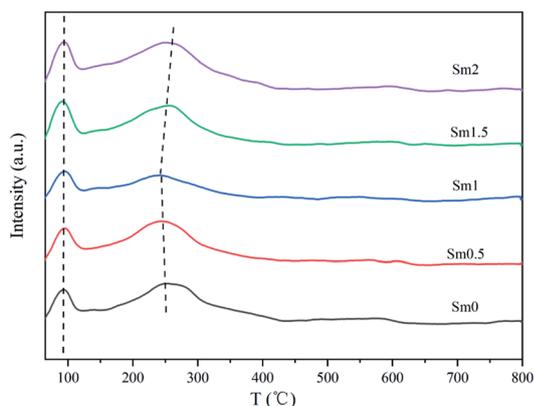

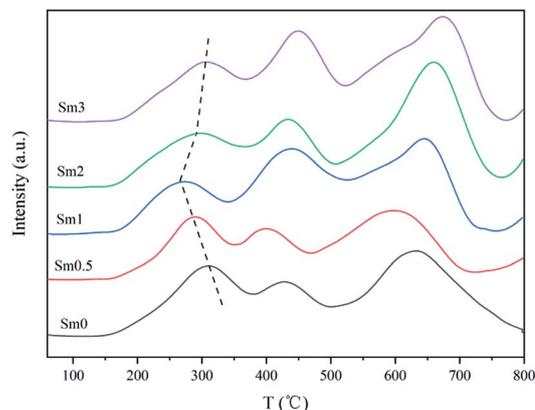**Fig. 4** H_2-TPD patterns of the FeMnSm catalysts with different Sm loadings.

Fig. 6 H_2-TPR patterns of the FeMnSm catalysts with different Sm loadings.
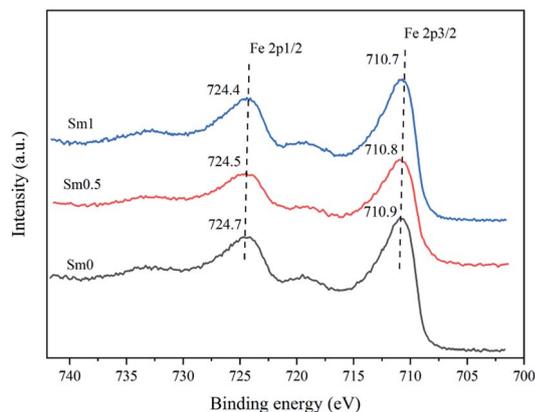
Fig. 7 XPS patterns of the FeMnSm catalysts with different Sm loadings.

atom with the increase in Sm. Previous studies have shown that higher surface electron densities will exhibit lower bond energies in XPS.[40] The electronegativity of Fe is higher than that of Sm. Therefore, the Sm atom would donate electrons to the Fe atom, resulting in Fe being the central atom with higher charge density. In this way, Sm as a promoter could be considered as a weak electron donor, which could accelerate the dissociation of adsorbed CO and decrease H_2 absorption,[34,41] resulting in a higher concentration of carbon species on the catalyst surface.

3.1.4. Phase composition of catalysts after reaction. The bulk iron phases in the Sm-promoted catalysts after the reaction were measured by Mössbauer spectroscopy (MES). The results are shown in Fig. 8. The MES parameters are listed in Table 2.

As shown in Table 2, the sextets with a hyperfine field (Hhf) of 487–490 and 453–455 kOe can be attributed to Fe_3O_4. The former represents the tetrahedron site (A site) in the Fe_3O_4 phase, and the latter represents the eight position sites (B site) in the Fe_3O_4
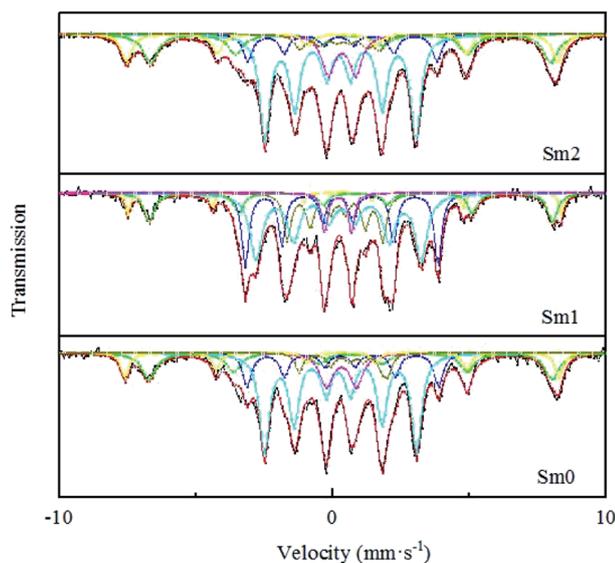

Fig. 8 Mössbauer spectra of the Sm-promoted catalysts after the reaction.

phase. The sextets with a hyperfine field (Hhf) of 214–218, 170–180 and 92–108 kOe could be attributed to χ-Fe_5C_2.[42] It is generally believed that Fe_5C_2 is the reactive phase of the FTS reaction.[43,44] Compared with the observation for the Sm-free catalyst, the content of Fe_5C_2 increased from 64.4% to 76.9% in the Sm1 catalyst based on the BET, CO-TPD and XPS studies. A possible explanation for this might be that a small amount of Sm could increase the dispersion of the iron-based catalyst, resulting in the increase in the Fe and CO binding sites.[45] Moreover, the strong electron interaction between Sm and Fe promoted CO adsorption and enhanced the Fe–C bond, leading to more Fe_5C_2 formation. However, in the Sm2 sample, the content of χ-Fe_5C_2 decreased to 60.4%, which may be related to the blockage of the catalyst pores, resulting in a decrease in the number of active sites of the catalysts. Meanwhile, similar conclusions were reached from BET and CO-TPD. Furthermore, the remaining iron phases could be considered as un-reduced Fe^{3+} with a small grain superparamagnetic (spm) state. The content of Fe^{3+} (spm) in the Sm1 sample was the lowest, which meant that the reduction degree of Sm1 was the highest and was consistent with the conclusion from H_2-TPR.

3.2. FTS performance

The activities and product distribution of the catalysts with different Sm loadings for FTS measured under the conditions of 300 °C, 1.0 MPa, 12 000 ml g^{-1} h^{-1} and $H_2/CO = 2$ in a fixed bed are shown in Table 3. According to the results, the CO conversion for the catalysts increased from 63.4% to 70.4% with the increase in the Sm loading from 0 to 1%. It is possible that these results were due to a combination of various factors. First, the BET surface area increased with the introduction of a small amount of Sm, and the large BET surface area provided more active sites, leading to higher CO conversion. Second, according to H_2-TPR, the lowest first peak temperature for the sample Sm1 meant that it was the easiest to reduce to Fe_3O_4 and then convert to Fe_5C_2, which was also reflected in MES. Lastly, the results of XPS and CO-TPD showed that the addition of an appropriate amount of Sm can increase the electron density of the Fe surface, promoting CO adsorption as well as enhancing the formation of the Fe–C bonds. This benefited the generation of Fe_5C_2, as confirmed by MES, resulting in higher activity.[46,47] When the Sm content increased from 1% to 2%, CO conversion decreased, which may be due to the decrease in the BET surface area. In this way, the number of active sites decreased. Meanwhile, the introduction of excessive Sm was not conducive to the reduction of the catalysts. Both factors hindered CO adsorption and inhibited iron carbide formation, finally leading to low FTS activity.[48]

The FTS product selectivity of the catalysts with different Sm loadings and their detailed data are also listed in Table 3. The catalysts presented selectivity of $C_{2-4}^=$ in the HC distribution, which increased from 26.6% to 32.6% after the addition of samarium from 0 to 1%, but it decreased to 27.7% as the Sm amount continued to increase to 2%. Research studies have shown that the formation of low-carbon olefins is related to the basicity of the catalyst surface.[49,50] In short, increasing the surface basicity in the FTS catalyst can suppress H_2 adsorption.

Table 2 MES parameters of the Sm-promoted catalysts after the reaction[a]

Catalyst	Assignment	Hhf (kOe)	IS (mm s^{-1})	QS (mm s^{-1})	Γ/2 (mm s^{-1})	Area (%)
Sm0	Fe^{3+}(spm)		0.30	1.09	0.29	9.3
	Fe_3O_4(A)	489.17	0.32	−0.02	0.18	9.1
	Fe_3O_4(B)	454.49	0.63	0.00	0.32	17.2
	χ-Fe_5C_2	215.84	0.30	−0.11	0.20	13.6
		171.34	0.23	−0.09	0.22	44.0
		100.00	0.61	0.45	0.17	6.8
Sm1	Fe^{3+}(spm)		0.21	0.98	0.13	3.8
	Fe_3O_4(A)	488.10	0.30	−0.24	0.10	4.8
	Fe_3O_4(B)	454.56	0.73	0.16	0.22	13.2
	χ-Fe_5C_2	217.10	0.25	−0.14	0.15	23.8
		175.96	0.26	0.10	0.27	36.7
		107.5	0.13	0.10	0.17	16.4
Sm2	Fe^{3+}(spm)		0.35	0.98	0.23	9.7
	Fe_3O_4(A)	487.65	0.32	−0.01	0.23	11.8
	Fe_3O_4(B)	453.21	0.65	0.02	0.35	18.2
	χ-Fe_5C_2	214.18	0.27	−0.13	0.22	10.6
		170.85	0.23	−0.08	0.23	43.4
		92.45	0.34	0.11	0.21	6.4

[a] Reaction condition: 300 °C, H_2/CO = 2, 1.0 MPa and 12 000 ml g^{-1} h^{-1}.

Table 3 Catalyst performance of the FeMnSm catalysts with different Sm loadings[a]

Catalyst	CO conversion (%)	CO$_2$ selectivity (%)	HC distribution (%)				O/P
			C$_1$	C$_{2-4}$$^=$	C$_{2-4}$^{0}	C$_5^+$	
Sm0	63.4	43.5	13.9	26.6	6.5	52.9	4.09
Sm0.5	68.4	45.6	15.1	28.9	7.0	48.8	4.13
Sm1	70.4	49.3	15.4	32.6	7.8	44.0	4.18
Sm1.5	64.2	45.4	16.7	28.7	9.0	45.4	3.19
Sm2	48.8	45.0	16.0	27.2	8.9	47.7	3.06

[a] Reduction conditions: T = 350 °C, P = 0.1 MPa, 4000 ml g^{-1} h^{-1}, H_2, TOS = 10 h. Reaction conditions: T = 300 °C, P = 1.0 MPa, 12 000 ml g^{-1} h^{-1}, H_2/CO = 2.

The H_2-TPD and CO_2-TPD results indicated that the catalyst surface basicity increased, while the H_2 concentration on the catalyst surface decreased from sample Sm0 to Sm1; however, this trend changed in the opposite direction from sample Sm1 to Sm2. Strong alkalinity and lower hydrogen adsorption properties inhibited the hydrogenation reaction, which suppressed the conversion of olefins to paraffins. Therefore, sample Sm1 with the strongest basicity and the weakest hydrogen adsorption showed the highest selectivity of $C_{2-4}^=$ and the ratio of olefins to paraffins (O/P). In addition, the selectivity of C_{5+} was negatively correlated with conversion, which was consistent with the results reported in the literature.[51,52]

4. Conclusions

The Sm-promoted FeMn catalysts were prepared by the co-precipitation method and their performance was investigated in a fixed bed reactor. It was found that the highly selective production of light olefins can be achieved at higher activities over the FeMn catalysts promoted by a proper amount of Sm. In regard to the catalyst texture, Sm introduced into the samples could increase

the BET surface areas, pore volumes and the formation of Fe particles with a smaller size. The presence of Sm could enhance the dissociated adsorption of CO and inhibit the adsorption of H_2. Furthermore, the electron transfer between samarium and iron helped increase the surface charge density of the iron atoms, as confirmed by XPS. Sm could also promote the formation of Fe_5C_2, leading to high FTS activity. In addition, the introduction of an appropriate amount of Sm enhanced the basicity of the catalysts and inhibited the hydrogenation reaction, leading to the formation of more light olefins. As a result, the Sm1 sample exhibited 70.3% CO conversion, 32.6% $C_{2-4}^=$ yield and O/P ratio of 4.18 at 300 °C, 1.0 MPa and WHSV of 12 000 ml g^{-1} h^{-1}.

Conflicts of interest

There are no conflicts to declare.

Notes and references

1 V. Garcilaso, J. Barrientos, L. F. Bobadilla, O. H. Laguna, M. Boutonnet, M. A. Centeno and J. A. Odriozola, *Renewable Energy*, 2019, **132**, 1141–1150.

2 M. Janardanarao, *Ind. Eng. Chem. Res.*, 1990, **29**, 1735–1753.

3 H. Schulz, *Appl. Catal., A*, 1999, **186**, 3–12.

4 T. T. Lari, *RSC Adv.*, 2017, **7**, 34497–34507.

5 F. Tihay, A. C. Roger, A. Kiennemann and G. Pourroy, *Catal. Today*, 2000, **58**, 263–269.

6 B. Liu, W. Li, J. Zheng, Q. Lin and X. Liu, *Catal. Sci. Technol.*, 2018, **8**, 5288–5301.

7 W. Ngantsouehoc, Y. Q. Zhang, R. J. O'Brien, M. S. Luo and B. H. Davis, *Appl. Catal., A*, 2002, **236**, 77–89.

8 M. Luo, B. H. Davis and H. Burtron, *Appl. Catal., A*, 2003, **246**, 171–181.

9 Y. Xu, X. Jia and X. Liu, *Catal. Sci. Technol.*, 2018, **8**, 1953–1970.

10 F. Morales, E. de Smit, F. M. de Groot, T. Visser and B. M. Weckhuysen, *J. Catal.*, 2007, **246**, 91–99.

11 J. B. Li, H. F. Ma, H. T. Zhang, Q. W. Sun, W. Y. Ying and D. Y. Fang, *Fuel Process. Technol.*, 2014, **125**, 119–124.

12 M. Feyzi, M. Irandoust and A. A. Mirzaei, *J. Fuel Chem. Technol.*, 2012, **40**, 550–557.

13 M. Feyzi, M. Irandoust and A. A. Mirzaei, *Fuel Process. Technol.*, 2011, **92**, 1136–1143.

14 N. Lohitharn, J. G. Goodwin and E. Lotero, *J. Catal.*, 2008, **255**, 104–113.

15 N. Lohitharn and J. G. Goodwin Jr, *J. Catal.*, 2008, **257**, 142–151.

16 H. Wang, Y. Yong, X. U. Jian, W. Hong, M. Ding and Y. Lia, *J. Mol. Catal. A: Chem.*, 2010, **326**, 29–40.

17 Ö. F. Gül, Ö. Ataç, İ. Boz and Ş. Özkara-Aydınoğlu, *React. Kinet., Mech. Catal.*, 2016, **117**, 147–159.

18 Y. Yang, H. W. Xiang, L. Tian, H. Wang, C. H. Zhang, Z. C. Tao, Y. Y. Xu, B. Zhong and Y. W. Li, *Appl. Catal., A*, 2005, **284**, 105–122.

19 H. N. Pham and A. K. Datye, *Catal. Today*, 2000, **58**, 233–240.

20 H. Wan, B. Wu, C. Zhang, B. Teng and Z. TAO, *Fuel*, 2006, **85**, 1371–1377.

21 V. P. Santos, L. Borges, S. Sartipi, B. V. D. Linden, A. I. Dugulan, A. Chojecki, T. Davidian, M. Ruitenbeek, G. R. Meima and F. Kapteijn, *Appl. Catal., A*, 2017, **533**, 38–48.

22 D. Z. Wang, X. P. Cheng, Z. E. Huang, X. Z. Wang and S. Y. Peng, *Appl. Catal.*, 1991, **77**, 109–122.

23 W. Han, L. Wang, Z. Li, H. Tang, Y. Li, C. Huo, G. Lan, X. Yang and H. Liu, *Appl. Catal., A*, 2019, **572**, 158–167.

24 X.-L. Zhou, G. P. Felcher and S.-H. Chen, *Phys. B*, 1991, **173**, 167–179.

25 L. Zhao, G. Liu and L. I. Jinlin, *Chin. J. Catal.*, 2009, **30**, 637–642.

26 W. Qian, H. Zhang, W. Ying and D. Fang, *J. Nat. Gas Chem.*, 2011, **20**, 389–396.

27 M. Thommes, K. Kaneko, A. V. Neimark, J. P. Olivier, F. Rodriguez-Reinoso, J. Rouquerol and K. S. Sing, *Pure Appl. Chem.*, 2015, **87**, 1051–1069.

28 C.-I. Ahn and J. W. Bae, *Catal. Today*, 2016, **265**, 27–35.

29 F. J. Pérez-Alonso, T. Herranz, S. Rojas, M. Ojeda, M. López Granados, P. Terreros, J. L. G. Fierro, M. Gracia and J. R. Gancedo, *Green Chem.*, 2007, **9**, 663–670.

30 J. B. Li, H. F. Ma, H. T. Zhang, Q. W. Sun, W. Y. Ying and D. Y. Fang, *Acta Phys.-Chim. Sin.*, 2014, **30**, 1932–1940.

31 S. K. Das, P. Mohanty, S. Majhi and K. K. Pant, *Appl. Energy*, 2013, **111**, 267–276.

32 M. E. Dry, T. Shingles and C. S. V. H. Botha, *J. Catal.*, 1970, **17**, 341–346.

33 C. Nie, H. Zhang, H. Ma, W. Qian, Q. Sun and W. Ying, *Catal. Lett.*, 2019, 1–8.

34 C. Zhang, G. Zhao, K. Liu, Y. Yang, H. Xiang and Y. Li, *J. Mol. Catal. A: Chem.*, 2010, **328**, 35–43.

35 F. Bozso, G. Ertl, M. Grunze and M. Weiss, *Appl. Surf. Sci.*, 1977, **1**, 103–119.

36 X. Gao, J. Zhang, N. Chen, Q. Ma, S. Fan, T. Zhao and N. Tsubaki, *Chin. J. Catal.*, 2016, **37**, 510–516.

37 R. A. Dictor and A. T. Bell, *J. Catal.*, 1986, **97**, 121–136.

38 I. R. Leith and M. G. Howden, *Appl. Catal.*, 1988, **37**, 75–92.

39 T. Yamashita and P. Hayes, *Appl. Surf. Sci.*, 2008, **254**, 2441–2449.

40 S. Qin, C. Zhang, J. Xu, Y. Yang, H. Xiang and Y. Li, *Appl. Catal., A*, 2011, **392**, 118–126.

41 J. Huang, W. Qian, H. Zhang and W. Ying, *Catal. Sci. Technol.*, 2017, **7**, 5530–5539.

42 M. H. Mahmoud, H. H. Hamdeh, J. C. Ho, M. J. O'Shea and J. C. Walker, *J. Magn. Magn. Mater.*, 2000, **220**, 139–146.

43 G. V. D. Laan and A. A. C. M. Beenackers, *Catal. Rev.*, 1999, **41**, 255–318.

44 M. E. Dry, *Catal. Today*, 2002, **71**, 227–241.

45 C. Yang, H. Zhao, Y. Hou and D. Ma, *J. Am. Chem. Soc.*, 2012, **134**, 15814–15821.

46 T. H. Pham, X. Duan, Q. Gang, X. Zhou and D. Chen, *J. Phys. Chem. C*, 2014, **118**, 37–49.

47 J. Feng, Z. Min, L. Bing, Y. Xu and X. Liu, *Catal. Sci. Technol.*, 2017, **7**, 1245–1265.

48 B. Liu, S. Geng, J. Zheng, X. Jia, F. Jiang and X. Liu, *ChemCatChem*, 2018, **10**, 4718–4732.

49 Q. Chen, W. Qian, H. Zhang, H. Ma, Q. Sun and W. Ying, *Catal. Commun.*, 2019, 4718–4732.

50 A. N. Pour, S. M. K. Shahri, H. R. Bozorgzadeh, Y. Zamani, A. Tavasoli and M. A. Marvast, *Appl. Catal., A*, 2008, **348**, 201–208.

51 J. L. Rankin and C. H. Bartholomew, *J. Catal.*, 1986, **100**, 526–532.

52 J. L. Rankin and C. H. Bartholomew, *Cheminform*, 1986, **100**, 533–540.